

1 The Kuroshio Extension: A Leading Mechanism for the Seasonal Sea-level Variability along the West  
2 Coast of Japan

3  
4 Chao Ma<sup>1,2,3</sup>, Jiayan Yang<sup>3</sup>, Dexing Wu<sup>2</sup>, Xiaopei Lin<sup>2</sup>

5  
6 1. College of Physical and Environmental Oceanography

7 Ocean University of China

8 Qingdao 266100, China

9 2. Physical Oceanography Laboratory

10 Ocean University of China

11 Qingdao 266100, China

12 3. Department of Physical Oceanography

13 Woods Hole Oceanographic Institution

14 Woods Hole, MA 02543, USA

15  
16 Corresponding Author: Chao Ma ([machao@ouc.edu.cn](mailto:machao@ouc.edu.cn))

17 Abstract

18       Sea level changes coherently along the two coasts of Japan on the seasonal time scale. AVISO  
19 satellite altimetry data and OFES (OGCM for the Earth Simulator) results indicate that the variation  
20 propagates clockwise from Japan's east coast through the Tsushima Strait into the Japan/East Sea (JES)  
21 and then northward along the west coast. In this study, we hypothesize and test numerically that the sea  
22 level variability along the west coast of Japan is remotely forced by the Kuroshio Extension (KE) off the  
23 east coast. Topographic Rossby waves and boundary Kelvin waves facilitate the connection. Our 3-d  
24 POM model when forced by observed wind stress reproduces well the seasonal changes in the vicinity  
25 of JES. Two additional experiments were conducted to examine the relative roles of remote forcing and  
26 local forcing. The sea level variability inside the JES was dramatically reduced when the Tsushima Strait  
27 is blocked in one experiment. The removal of the local forcing, in another experiment, has little effect on  
28 the JES variability. Both experiments support our hypothesis that the open-ocean forcing, possibly  
29 through the KE variability, is the leading forcing mechanism for sea level change along the west coast of  
30 Japan.

31 1. Introduction

32 The Kuroshio and Oyashio Currents are two major western boundary currents (WBCs) in the North  
33 Pacific Ocean. Flowing toward each other along the continental slope off the Asian Marginal Seas, there  
34 is a mixed water region between the two off the coast of Honshu – the largest Japanese Island. The  
35 merged currents transport the WBCs water offshore and form the Kuroshio Extension (KE) (Talley et al.,  
36 1995; Qiu, 2003). The KE, like its counterpart the Gulf Stream Extension (GSE) in the North Atlantic  
37 Ocean, is a meandering current (Kawabe, 1995; Mitsudera et al., 2001, among others) with high eddy  
38 variability as observed by satellite altimeters (e.g., Qiu, 2000; Qiu and Chen, 2005). From the  
39 perspective of ocean dynamics, it is expected that the sea surface height (SSH) along the east coast of  
40 Honshu would be influenced directly by the KE variability because mesoscale eddies transport energy  
41 westward. Where does the KE-induced coastal variability propagate and how does it force remote  
42 regions, however, have been less examined. In this study, we will investigate the KE forcing of the  
43 seasonal SSH variability along the west coast of Honshu inside the Japan/East Sea (JES).

44 The JES is a deep semi-enclosed sea which is bounded by the Asian continent to the west and the  
45 Japanese Islands to the east. The Tsushima Warm Current (TSWC), which is generally considered as a  
46 branch of the Kuroshio, especially in winter, flows into the JES through the Tsushima Strait from the  
47 East China Sea. The water flows out of the JES into the Pacific Ocean through the Tsugaru Strait and  
48 into the Sea of Okhotsk through the Soya and Tartar Straits. The Tartar Strait is very narrow and shallow,  
49 and seasonally frozen. So the Tsushima, Tsugaru and Soya Straits are the main passages for the JES  
50 inflow and outflow.

51 As for variability inside the JES, most of the previous studies focused on local forcing (Seung and  
52 Yoon, 1995; Teague et al., 2005) and on the transport of the TSWC (Isobe et al., 1994; Teague et al.,  
53 2002; Takikawa et al., 2005). In addition, variability in the Pacific Ocean would inevitably affect the  
54 TSWC and the JES (e.g., Lyu and Kim, 2003). SSH interannual variability within the JES is in phase  
55 with the Pacific Decadal Oscillation via the Kuroshio (Gordon and Giulivi, 2004). The TSWC is forced  
56 by the Subtropical and Subpolar Gyres in the North Pacific Ocean (Yang et al., 2006).

57 In this study, we will demonstrate that the seasonal variability along the west coast of Honshu is  
58 remotely forced by the KE variability and topographic Rossby waves, and boundary-trapped Kelvin  
59 waves may be responsible for this connection. The time evolution of the SSH along the Honshu coast  
60 from satellite altimetry data (AVISO, 2008) indicate that the signal of anomalous SSH appeared  
61 coherently along the coast from the KE area into the JES (Figure 1a). To show the linkage we chose a  
62 grid between 148°-150°E, 34°-36°N, which located in the KE region, and two tidal stations-Kushima  
63 and Hamada, which are located in the east and west coast of Honshu respectively and marked in Figure  
64 1a. The SSH variability averaged from AVISO data in the grid and measured at these two stations varied  
65 coherently from intra-seasonal to interannual time scales (Figure 2), indicating that the variability at KE  
66 region and these two stations may indeed be related to each other. The correlation coefficient of the two  
67 stations is 0.722 and above the 99% confidence level. But there is not significant phase lag, which may  
68 attribute to the rapid signal propagation and 1-month data interval.

69 In this study, we will analyze AVISO altimetry data and OFES (OGCM for the Earth Simulator)  
70 results, and use a three-dimensional model to examine whether the KE variability remotely forces the

71 seasonal SSH variability along the west coast of Honshu. The paper is organized as follows: the data and  
72 model results will be presented in section 2, and discussed and summarized in section 3.

73

## 74 2. Data analyses and model simulations

75 Satellite altimetry has played an increasingly important role in observing variability of the global  
76 sea level, and the altimeter data have been widely utilized in examining the spatial scales, generation  
77 mechanisms, propagation and kinetic energy distributions of various oceanic modes of variability (e.g.,  
78 Ichikawa and Imawaki, 1994; Fu and Chelton, 2001; Fu and Qiu, 2002). The newly merged product of  
79 altimeter data (AVISO, 2008) provides observations of SSH variations since October 1992, with a  
80 relatively high spatial resolution ( $1/4^\circ$  by  $1/4^\circ$ ) at short time intervals (7 days). In this study, we are  
81 primarily interested in the seasonal variability and so we have compiled a monthly climatology based on  
82 the 7-day AVISO data. Figure 1a shows the SSH deviation in September. The sea level in the whole  
83 eastern JES and particularly along the west coast of the Japanese Islands, from Kyushu to Hokkaido, is  
84 seasonally higher than the annual mean (which is removed in Figure 1a). The high SSH apparently  
85 extends to the southeastern coast of Japan. Interestingly, there are two large anti-cyclones with high SSH  
86 to the east of Japan, one in the KE region at  $146^\circ\text{E}$ ,  $35^\circ\text{N}$  and the other off Kyushu Island at  $135^\circ\text{E}$ ,  
87  $30^\circ\text{N}$ .

88 The OFES model, described in detail by Masumoto et al. (2004), is based on the MOM3 with a  
89 horizontal grid spacing of  $1/10^\circ$ . It was run starting from the World Ocean Atlas 1998 annual mean for  
90 more than 50 model years, forced by monthly mean wind stresses averaged from 1950 to 1999 from the

91 NCEP/NCAR reanalysis data (Sasaki et al., 2004; 2007). The high resolution and realistic coastline of  
92 OFES data could improve the understanding of the SSH variability around the Japanese Islands. The  
93 fifteen years (1990-2004) output of 3-day snapshots of the SSH are used in this study, which is  
94 comparable with the time span of altimetry data. We also removed annual mean and compiled a monthly  
95 climatology based on the OFES data. Figure 1b shows the SSH deviation in September as well. And the  
96 result is consistent with that from altimeter data: there is high sea level all the way from the southeastern  
97 coast to the western coast of Japan through the Tsushima Strait.

98 To examine whether the high SSH along the two coasts of Japan are related to each other, we drew  
99 a temporal-spatial section of sea level anomaly along PV contour near the coast of Japanese Islands as  
100 marked from A to E in Figure 3a. There is a distinct seasonal change of the SSH around the Honshu and  
101 Kyushu Islands (Figure 3b is from AVISO altimetry data, Figure 3c is from OFES results). The change  
102 appears to be coherent along the entire coastline. The sea level is high in the late summer and early fall  
103 around September and October, and low in the late winter in March. There is a clear indication from  
104 these two figures that seasonal SSH anomaly propagates clockwise starting from A, though B and C  
105 along the southern coast of Honshu Island, then pass D to E along the west coast of Honshu Island. The  
106 phase lags between sea level variations at station pairs of A and B, B and C, and C and D are nearly 1  
107 week, and the correlation coefficient passed 95% confidence level. The time scale of the propagation  
108 around one path shown in Figure 3a is roughly one month and the speed is about 1.5 m/s.

109 We estimated theoretical coastal Kelvin wave and topographic Rossby wave speed. Here, we used  
110 the long Rossby wave approximation in calculation of the phase speed (Pedlosky, 1979),

111

$$c_K = \sqrt{g'h}$$

112

$$c_R = -(\beta + \frac{f}{h}s)R_d^2$$

113

114

115

116

117

where  $g'$  is the reduced gravity,  $h$  is the water depth,  $s$  is the bottom slope,  $R_d$  is Rossby deformation radius. In application to Japan Islands,  $\beta = 1.9 \times 10^{-11} m^{-1} s^{-1}$ ,  $f = 8.3 \times 10^{-5} s^{-1}$  (the latitude is  $35^\circ N$ ),  $g' = g \times 1e^{-3}$ ,  $h \approx 1000m$ ,  $s \approx 0.1$ . Thus, the theoretical Kelvin wave speed is about 3.1 m/s, while the theoretical topographic Rossby wave speed is about 1.2 m/s, which is more comparable with the satellite observation.

118

119

120

121

122

123

124

125

126

In order to examine the mechanism of seasonal variability along Japan's coast, a 3-D full forcing model was used. The model is the latest version of the Princeton Ocean Model (POM). The simulation domain is  $100^\circ$ - $150^\circ E$ ,  $0^\circ$ - $50^\circ N$  with a resolution of  $1/6^\circ$  by  $1/6^\circ$  horizontally, and 16 sigma levels vertically. The bathymetry used in the model is interpolated from ETOPO5 5-minute gridded elevation data (NOAA, 1988). The model is initialized with temperature and salinity fields for January from the National Oceanographic Data Center (Levitus et al., 1994; Levitus and Boyer, 1994), and is forced by monthly mean climatologic atmospheric fields. The wind stress is from the National Center for Environmental Prediction (NCEP, Kistler et al., 2001). Along the boundaries, we specify model variables from the results of a global model (Qiao et al., 2004).

127

128

129

130

In the standard run, the model was integrated for 10 years until it reached a statistically steady seasonal cycle. The spin-up time scale for a baroclinic ocean with the size of the Pacific is much longer than 10 years, especially in higher latitudes within the model domain. The relatively short spin-up time in our model integration is due to the use of a small model domain. The boundary condition prescribed

131 from a coarse-resolution global model already contains the spin-up information in the vast interior ocean.  
132 The main features of the circulations in the region are well simulated and consistent with  
133 observation-based description (Su, 2001). In this study, we will concentrate on the seasonal variability  
134 along the coast of Japan. The SSH deviation from the annual mean in the month of September is shown  
135 in Figure 4a. There are noticeable differences in the details between the model simulation (Figure 4a)  
136 and the altimetry data (Figure 1a) or the OFES results (Figure 1b). For instance, the anti-cyclone off  
137 Kyushu's coast is weaker in the model. But there is broad similarity between the model and data. The  
138 high SSH along Japan's coast is well simulated. The SSH anomaly pattern off the east coast of Japan is  
139 comparable with the data. We calculated the temporal-spatial evolution of SSH around Honshu and  
140 Kyushu from the model output (Figure 3d). The pattern is similar to that from the altimetry data (Figure  
141 3b) and OFES results (Figure 3c) except that the seasonal cycle is slightly ahead in the model than in the  
142 data. Overall, the results from the standard run are reasonably consistent with satellite observations. This  
143 gives us some confidence to use the model to examine mechanisms. Two additional experiments are  
144 designed here: (1) block the Tsushima Strait; (2) remove the local forcing of wind stress. The results will  
145 be compared with the standard run.

146 In the first sensitivity experiment, the Tsushima Strait is blocked and everything else remains  
147 unchanged from the standard run. The sea level anomaly of September is shown in Figure 4b. The most  
148 noticeable difference from the data (Figure 1) or our standard run (Figure 4a) is the absence of the high  
149 SSH along the west coast of Japan inside the JES. It should be noted here that the JES is still connected  
150 to the other basins through the Tsugaru and Soya Straits even though the Tsushima Strait is blocked in



151 this run. Both boundary Kelvin waves and topographic Rossby waves propagate clockwise around the  
152 Honshu and Kyushu Islands (a topographic Rossby wave in the northern hemisphere propagates along  
153 constant potential vorticity (PV) contours with a high PV or shallower bathymetry to its right hand side).  
154 So the variability originated along the east coast of Japan does not propagate directly into the JES  
155 through the Tsugaru Strait.

156 Another interesting feature in Figure 4b is that the high SSH along the west coast of Korea is  
157 heightened when the Tsushima Strait is blocked (compared Figure 4b and Figure 4a). When the  
158 Tsushima Strait is blocked, Kelvin and topographic Rossby waves cannot enter the JES and so they  
159 travel along the boundary into the Yellow Sea. This change further supports our hypothesis that wave  
160 propagation is responsible for the SSH changes along the west coast of Japan.

161 Next, we will examine the role of the local wind stress forcing. We remove the forcing within our  
162 model domain. The model is forced entirely by specifying the open-boundary conditions from a global  
163 run (Qiao et al., 2004). This represents the open-ocean forcing since the information from the vast  
164 interior is passed into the smaller domain through the open boundaries. The Kuroshio and Oyashio  
165 Currents, including the KE, remains robust since they are forced by the wind-stress curl in the vast  
166 interior ocean. The SSH anomaly in September (and all other months) is very similar to that from the  
167 standard run (Figure 4c vs. Figure 4a). This experiment demonstrates that the seasonal SSH variability  
168 along the west coast of Japan inside the JES is forced primarily by the open-ocean process instead of the  
169 local wind stress.

170

171 3. Discussion and Summary

172 Altimetry data and OFES results show that the SSH along the east and west coasts of Japan varies  
173 coherently with seasons, and indicate that the signal of such seasonal variability propagates clockwise  
174 from the southeastern coast of Honshu Island. This pattern was simulated well by a three-dimensional  
175 ocean model. In this study, we hypothesize and test that the seasonal SSH variability along the west  
176 coast of Japan inside the JES is forced remotely by the SSH changes along the east coast. The remote  
177 forcing is through topographic Rossby and/or boundary Kelvin waves, but much more prefer to the  
178 former according to the comparison between observed and theoretical values.

179 The open ocean responds to atmospheric forcing or adjusts to the internal oceanic interactions  
180 through the propagation of Rossby waves, eddies and meanders. These transient features typically move  
181 westward and would eventually feel the changing bathymetry as they approach the continental slope and  
182 shelf. In the absence of strong external forcing, they tend to move along the PV contours as topographic  
183 Rossby waves. In the northern hemisphere, they move in the direction with shallower bathymetry  
184 (higher PV) on their right hand side. In our application to the JES, topographic Rossby waves propagate  
185 clockwise around the Honshu and Kyushu Islands. Ageostrophic processes, such as friction, nonlinearity  
186 and external forcing, may force the flow to across the PV contours toward the land-sea boundary. So  
187 boundary Kelvin waves may also play a role in the remote forcing of SSH in JES.

188 Both the observation and models show mighty SSH variability in the KE region. So it may act as  
189 the energy source of remote forcing mentioned above. The KE has been considered to be an eastward  
190 inertial jet (Kawai, 1972; Yasuda et al., 1992) which is accompanied by large meanders and energetic

191 eddies. Due to its abundance of mesoscale eddy variability, the KE region is one of the regions with the  
192 highest eddy kinetic energy (Wyrтки et al., 1976). So the KE variability, as we hypothesize in this study,  
193 may be the leading mechanism for the seasonal SSH variability along the west coast of Japan inside the  
194 JES.

195 Acknowledgements

196 This work was conducted when Chao Ma was a visiting graduate student at WHOI. His visit has  
197 been supported by China Scholarship Council and WHOI Academics Office. This study has been  
198 supported by WHOI's Coastal Ocean Institute, the National Basic Research Program of China  
199 (2005CB422303 and 2007CB481804), the International Science and Technology Cooperation Program  
200 of China (2006DFB21250), the Natural Science Foundation of China (40706006) , and the Ministry of  
201 Education's 111 Project (B07036). Lin was supported by the Program for New Century Excellent  
202 Talents in University (NECT-07-0781).

203

204 References

- 205 AVISO (2008), *Ssalto/Duacs User Handbook: (M)SLA and (M)ADT Near-Real Time and Delayed Time*  
206 *Products*, SALP-MU-P-EA-21065-CLS, 32pp.
- 207 Fu, L.-L., and D. B. Chelton (2001), Large-scale ocean circulation, *Satellite Altimetry and Earth*  
208 *Sciences*, L.-L. Fu and A. Cazenava, Eds., Academic Press, 133–169.
- 209 Fu, L.-L., and B. Qiu (2002), Low-frequency variability of the North Pacific Ocean: The roles of  
210 boundary- and wind-driven baroclinic Rossby waves, *J. Geophys. Res.*, 107, 3220,  
211 doi:10.1029/2001JC001131.
- 212 Gordon, A.L. and C.F. Giulivi (2004), Pacific decadal oscillation and sea level in the Japan/East sea,  
213 *Deep-Sea Res. I*, 51, 653-663

214 Ichikawa, K. and S. Imawaki (1994), Life history of a cyclonic ring detached from the Kuroshio  
215 Extension as seen by the Geosat altimeter, *J. Geophys. Res.*, 99, 15,953–15,966.

216 Isobe, A., S. Tawara, A. Kaneko, and M. Kawano (1994), Seasonal variability in the Tsushima Warm  
217 Current, Tsushima-Korea Strait, *Cont. Shelf Res.*, 14, 23–35.

218 Kawabe, M. (1995), Variations of current path, velocity, and volume transport of the Kuroshio in  
219 relation with the large meander, *J. Phys. Oceanogr.*, 25, 3103–3117.

220 Kawai, H. (1972), Hydrography of the Kuroshio Extension, *Kuroshio: Its Physical Aspects*, H. Stommel  
221 and K. Yoshida, Eds., University of Tokyo Press, 235–354.

222 Kistler, R., and Coauthors (2001), The NCEP-NCAR 50-Year Reanalysis: Monthly Means CD-ROM  
223 and Documentation, *Bull. Amer. Meteor. Soc.*, 82, 247–268.

224 Levitus, S., and T. P. Boyer (1994), World Ocean Atlas 1994. Volume 4: Temperature, *NOAA Atlas*  
225 *NESDIS 4*, Washington, D. C., 117pp.

226 Levitus, S., R. Burgett, and T. P. Boyer (1994), World Ocean Atlas 1994. Volume 3: Salinity, *NOAA*  
227 *Atlas NESDIS 3*, Washington, D. C., 99pp.

228 Lyu, S. J., and K. Kim (2003), Absolute transport from the sea level difference across the Korea Strait,  
229 *Geophys. Res. Lett.*, 30, 1285–1288.

230 Masumoto, Y., H. Sasaki, T. Kagimoto, N. Komori, A. Ishida, Y. Sasai, T. Miyama, T. Motoi, H.  
231 Mitsudera, K. Takahashi, H. Sakuma, and T. Yamagata (2004), A fifty-year eddy-resolving  
232 simulation of the world ocean—Preliminary outcomes of OFES (OGCM for the Earth Simulator), *J.*

233 *Earth Simulator*, 1, 35–56.

234 Mitsudera, H., T. Waseda, Y. Yoshikawa, and B. Taguchi (2001), Anticyclonic Eddies and Kuroshio  
235 Meander Formation, *Geophys. Res. Lett.*, 28(10), 2025–2028.

236 NOAA (1988), Data Announcement 88-MGG-02, Digital relief of the surface of the Earth, *Tech. Rep.*,  
237 NOAA, National Geophysical Data Center, Boulder, CO, U.S.A.

238 Pedlosky, J. (1979), *Geophysical Fluid Dynamics*. Springer-Verlag, 624 pp.

239 Qiao, F., Y. Yuan, Y. Yang, Q. Zheng, C. Xia, and J. Ma (2004), Wave-induced mixing in the upper ocean:  
240 Distribution and application to a global ocean circulation model, *Geophys. Res. Lett.*, 31, L11303,  
241 doi:10.1029/2004GL019824.

242 Qiu, B. (2000), Interannual Variability of the Kuroshio Extension System and Its Impact on the  
243 Wintertime SST Field, *J. Phys. Oceanogr.*, 30, 1486–1502.

244 Qiu, B. (2003), Kuroshio Extension Variability and Forcing of the Pacific Decadal Oscillations:  
245 Responses and Potential Feedback. *J. Phys. Oceanogr.*, 33, 2465–2482.

246 Qiu, B., and S. Chen (2005), Variability of the Kuroshio Extension Jet, Recirculation Gyre, and  
247 Mesoscale Eddies on Decadal Time Scales, *J. Phys. Oceanogr.*, 35, 2090–2103.

248 Sasaki, H., Y. Sasai, S. Kawahara, M. Furuichi, F. Araki, A. Ishida, Y. Yamanaka, Y. Masumoto, and H.  
249 Sakuma (2004), A series of eddy-resolving ocean simulations in the world ocean - OFES (OGCM  
250 for the Earth Simulator) project, *Ocean '04 - MTS/IEEE Techno-Ocean '04: Bridges across the*  
251 *Oceans - Conference Proceedings*, 3, 1535–1541.

252 Sasaki, H., M. Nonaka, Y. Masumoto, Y. Sasai, H. Uehara, and H. Sakuma (2007), An eddy-resolving  
253 hindcast simulation of the quasi-global ocean from 1950 to 2003 on the Earth Simulator, in *High*  
254 *resolution numerical modelling of the atmosphere and ocean*, edited by K. Hamilton and W.  
255 Ohfuchi, Springer, New York, 157–185.

256 Seung, Y.-H., and J.-H. Yoon (1995), Some features of winter convection in the Japan Sea, *J. Oceanogr.*,  
257 51, 61–73.

258 Su, J. (2001), A review of circulation dynamics of the coastal oceans near China (in Chinese with  
259 English abstract), *Acta Oceano. Sinica*, 23(4), 1–16.

260 Talley, L.D., Y. Nagata, M. Fujimura, T. Iwao, T. Kono, D. Inagake, M. Hirai, and K. Okuda (1995),  
261 North Pacific Intermediate Water in the Kuroshio/Oyashio Mixed Water Region, *J. Phys. Oceanogr.*,  
262 25, 475–501.

263 Teague, W.J., G.A. Jacobs, H.T. Perkins, J.W. Book, K.I. Chang, and M.S. Suk (2002), Low-Frequency  
264 Current Observations in the Korea/Tsushima Strait, *J. Phys. Oceanogr.*, 32, 1621–1641.

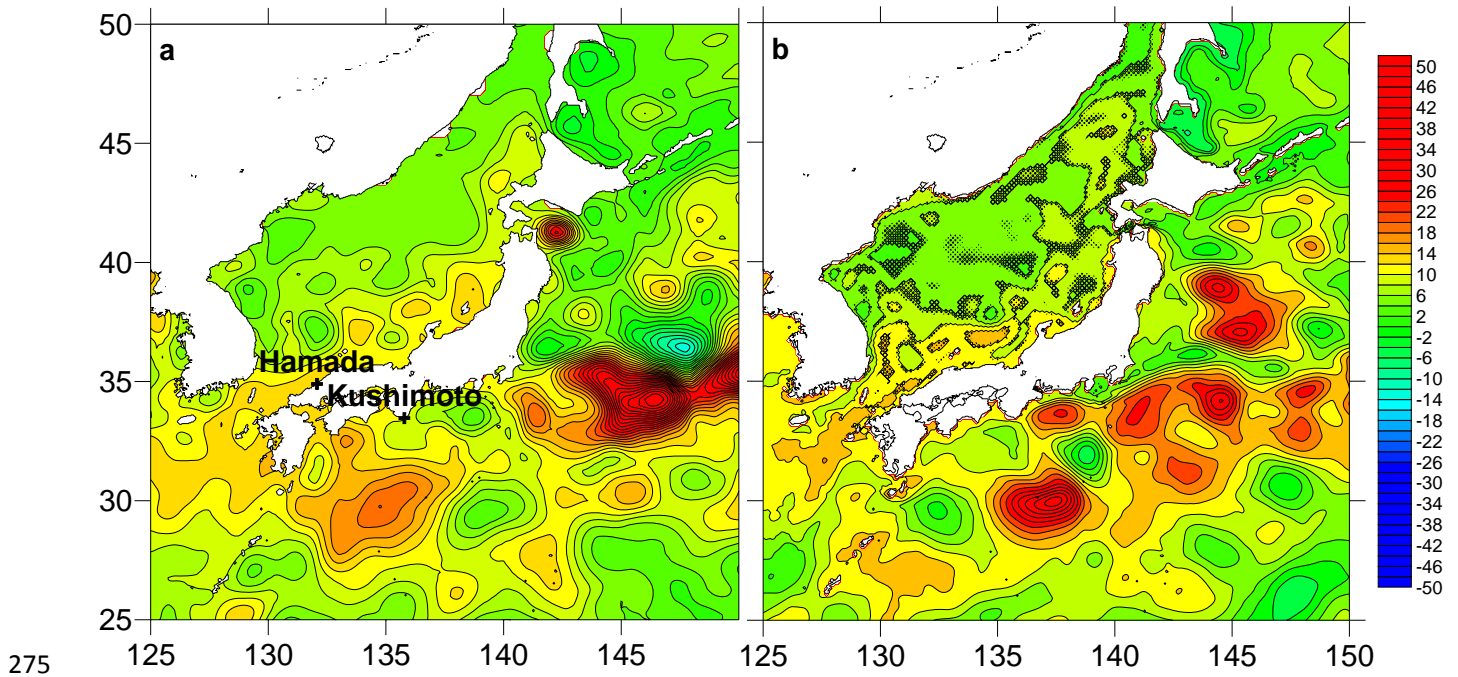
265 Teague, W. J., and Coauthors (2005), Observed deep circulation in the Ulleung Basin, *Deep-Sea Res. II*,  
266 52, 1802–1826.

267 Takikawa, T., J.-H. Yoon, and K.-D. Cho (2005), The Tsushima Warm Current through Tsushima  
268 Straits Estimated from Ferryboat ADCP Data, *J. Phys. Oceanogr.*, 35, 1154–1168.

269 Wyrtki, K., L. Magaard, and J. Hagar (1976), Eddy energy in the ocean, *J. Geophys. Res.*, 81,  
270 2641–2646.

- 271 Yang, J. (2006), The Kuroshio Forcing of Tsushima and Yellow Sea Warm Currents, *Eos Trans. AGU*,  
272 87(36), West. Pac. Geophys. Meet. Suppl., Abstract OS42A-07.
- 273 Yasuda, I., K. Okuda, and M. Hirai (1992), Evolution of a Kuroshio warm-core ring - Variability of the  
274 hydrographic structure, *Deep-Sea Res.*, 39(1A), S131–S161.





275

276 Figure 1: The September deviation of SSH from the annual mean (the contour interval is 2 cm).

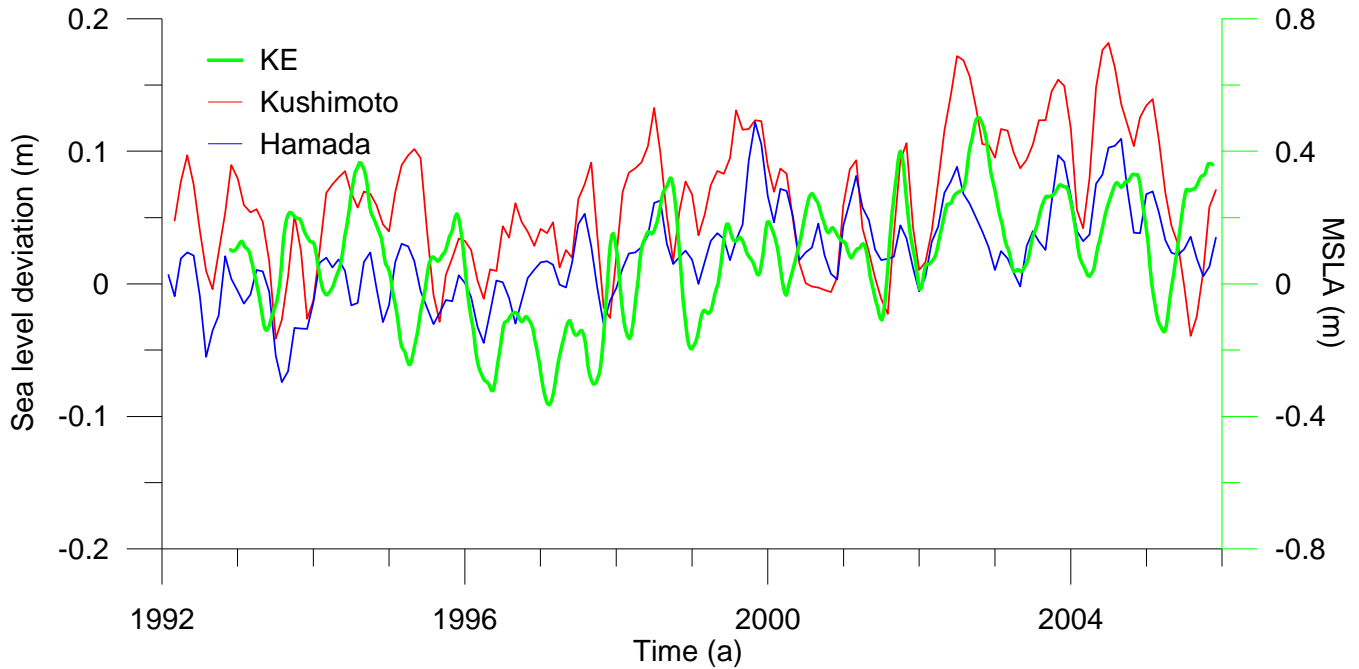
277 The left panel is from AVISO MSLA data and the right is from OFES results. The SSH along the entire

278 west coast of Japan inside the JES is seasonally high and appears to be related to the positive anomaly

279 along the southeast coast of Japan. This correlation of the SSH variability on two Japanese coasts is

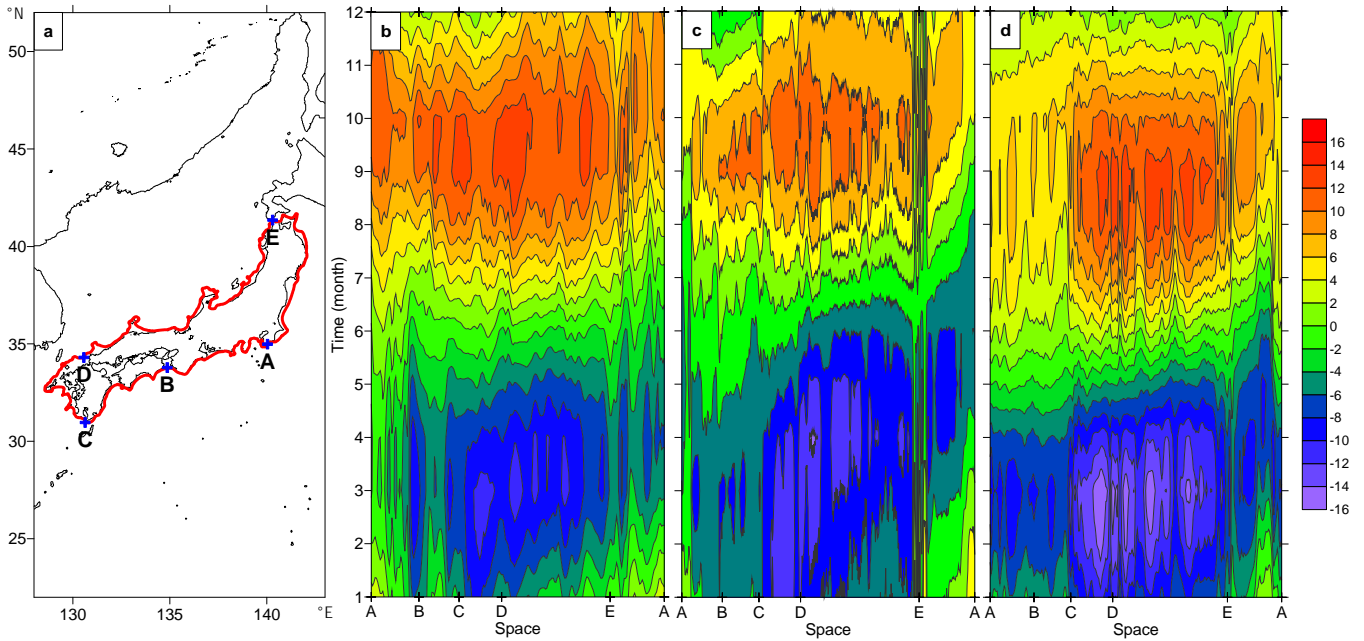
280 strong for the whole annual cycle as to be discussed later. Sea level data from two tidal stations at

281 Hamada and Kushimoto, as marked in the Figure, will be used in the following analyses.



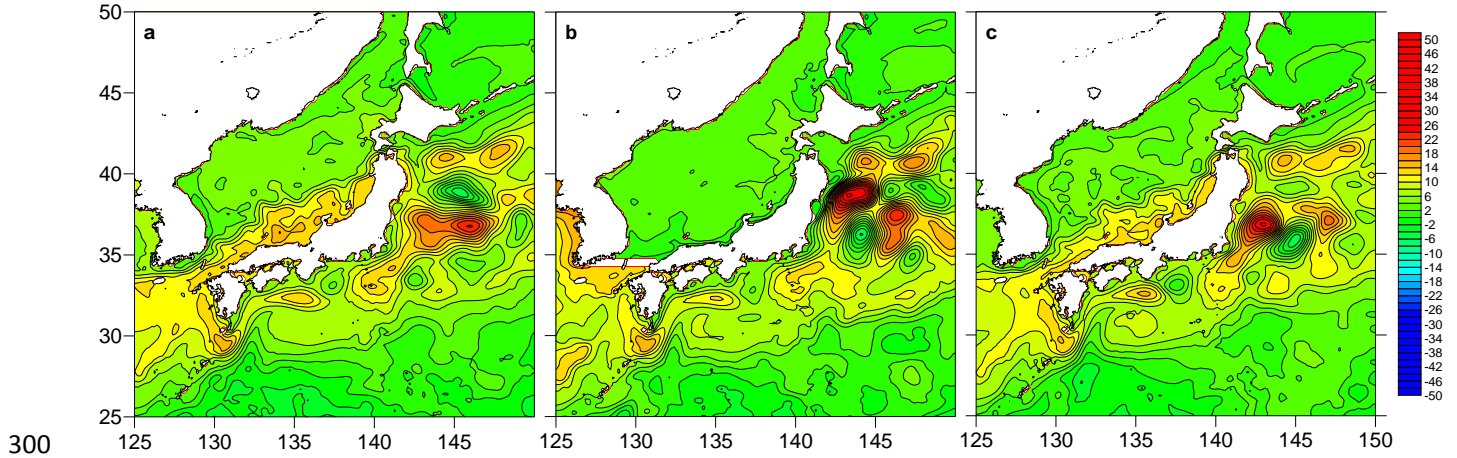
282

283 Figure 2: Monthly SSH anomaly averaged from AVISO data in the KE region (148°-150°E,  
 284 34°-36°N) and SSH deviation from the 15-year (1992-2006) mean measured at two tidal stations,  
 285 marked in Figure 1a. The left axis is for SSH deviation at the two tidal stations and the right is for SSH  
 286 averaged over KE region. A 6-month running mean is used to remove high-frequency variations. Both  
 287 stations showed upward trends. They were associated with global sea-level rise and beyond the scope of  
 288 this study. We are interested in the seasonal and interannual changes which were coherent at KE region  
 289 and these two stations. It indicates that the sea-level variability along the two coasts of Japan is likely  
 290 related.



291

292 Figure 3: To investigate the relationship of variability along two coasts of Japan, we plot the time  
 293 evolution of the seasonal SSH anomaly clockwise from the east coast of Japan at about 35°N. The path  
 294 is the PV contour ( $8 \times 10^{-6} \text{ m}^{-1} \text{ s}^{-1}$ ), and the direction is ABCDEA, as marked in the Figure 3a. The Figure  
 295 3b is from the altimetry data and clearly shows the clockwise propagation of SSH anomaly around  
 296 Honshu and Kyushu Islands. The Figure 3c is from OFES results and also shows the clockwise  
 297 propagation of SSH anomaly. The similar pattern of propagation was reproduced by the model except  
 298 that there is 1-month lead of the seasonal cycle in the model (Figure 3d) as compared to altimetry data.  
 299 The contour interval of SSH anomaly is 2 cm.



300  
 301 Figure 4: In addition to the standard run, two sensitivity experiments were conducted to test the  
 302 connectivity of the SSH variations between two Japanese coasts. The left panel is the monthly SSH  
 303 deviation in September from the standard run. It compares well with the altimetry data and OFES results  
 304 shown in Figure 1. In the first sensitivity experiment, the Tsushima Strait is blocked and everything else  
 305 remains unchanged. The SSH variability along the west coast of Japan virtually removed (middle panel),  
 306 indicating strongly that the SSH variability there is transmitted through the Tsushima Strait. In the  
 307 second sensitivity experiment, the local forcing within the model domain is removed and the model is  
 308 forced by the open boundary conditions from a coarser and basin-scale model. The SSH variability  
 309 along the west coast of Japan is robust even though there is no direct forcing within the JES (right panel).  
 310 This further supports our remote-forcing hypothesis.